ACS APPLIED MATERIALS & INTERFACES

Research Article

www.acsami.org

Ag@Fe_2O_3-GO Nanocomposites Prepared by a Phase Transfer Method with Long-Term Antibacterial Property

Nan Gao,[†,‡,§] Yingjie Chen,[†] and Jiang Jiang*[,†]

[†]i-Lab and Division of Nanobiomedicine, Suzhou Key Laboratory of Nanobiomedical Characterization, Suzhou Institute of Nano-tech and Nano-bionics, Chinese Academy of Sciences, Suzhou, China 215123

[‡]Graduate University of Chinese Academy of Sciences, Beijing, China 100049

[§]Institute of Chemistry, Chinese Academy of Sciences, Beijing, China 100190

Supporting Information

ABSTRACT: Silver has been utilized as a highly effective and broad-spectrum antibacterial agent in our daily life. However, low stability, poor long-term antibacterial efficiency, and potential environmental hazard of released Ag^+ ions may limit its practical applications. Ag-graphene oxide (GO) nanocomposites have been reported to display highly enhanced antibacterial property, yet their stability and long-term antibacterial properties have not been carefully investigated. Herein, we report the synthesis of Ag@Fe_2O_3-GO nanocomposites with tunable loading density up to full monolayer coverage by adopting a simple phase transfer method. Compared to Ag@Fe_2O_3, its GO composite shows enhanced stability with Ag^+ releasing rate decreased by more than two times under dialysis condition. We discover that the presence of GO not only slows down Ag nanoparticle oxidation process but also enables Ag^+ ions recrystallization on GO surface. The Ag@Fe_2O_3-GO nanocomposites have shown better and long-term antibacterial property against both Gram-negative and Gram-positive bacteria than those of plain Ag and Ag@Fe_2O_3, displaying great potential as a promising long-term bactericide with suppressed environmental hazard.

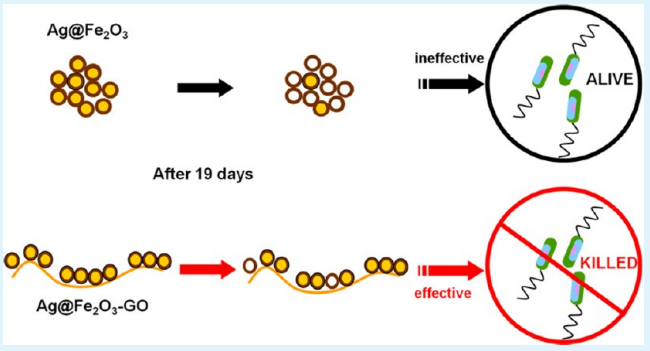

KEYWORDS: *antibacterial, core−shell nanoparticle, nanocomposite, hybrid, silver-graphene oxide, suppressed Ag release*

1. INTRODUCTION

Bacteria are microorganisms that can cause deadly infections. Thus, antibacterial materials are of great importance and necessity in our daily life. Other than commonly used antibiotics, nanomaterials including silver, copper, and some other metal or metal-based materials are also efficient bacteriostasis agents.[1] Among them, silver is the most widely investigated material. As a broad-spectrum antimicrobial agent, silver metal, silver salt, silver clusters or nanoparticles (NPs), and silver-based nanocomposites (NCs) can all be utilized as bactericides.[2−4] Several possible mechanisms have been proposed for the action of Ag on bacteria. One is that Ag nanomaterials release Ag^+ ions,[5,6] which can then bind to the thiol groups of bacterial enzymes and interfere with DNA replications. Particle-specific interaction of Ag NPs with bacteria, their subsequent penetration, and locally releasing Ag^+ ions causing bacteria death has also been proposed to account for their antibacterial property.[7−10] Another possible mechanism includes the oxidative stress generated by the formation of reactive oxygen species (ROS) at the surface of the Ag NPs.[6,11] Although the antibacterial mechanism of silver is not fully understood yet, its antimicrobial activity has been attributed mainly to the released Ag^+ ions.[5] Under ambient conditions, silver nanoparticles can be easily oxidized and release Ag^+ ions,[12] which would severely impair their stability and use in long-term antibacterial applications and allow them to become a potential environmental hazard.

Graphene (GR), first discovered in 2004, is a promising two-dimensional (2D) carbon material for a wide range of application areas including electronics,[13,14] energy,[15] catalysis,[16−20] and biosensing,[21−23] etc. At the same time, its derivative graphene oxide (GO), possessing abundant oxygen-containing functional groups (such as epoxy, hydroxyl, and carboxyl groups), enables its biomedical applications in drug delivery,[24,25] biosensing,[26] photothermal therapy,[27,28] and so forth. Nowadays, GO based nanocomposites are the research hotspots because of their ease of scale-up production[29] and potential synergistically enhanced effect. GO based hybrid materials inherit excellent physical and chemical properties from GO, as well as the specific properties of the supported NPs; thus, they are showing great potential in various fields such as biomedical, energy, and catalytic applications.[30−32] To

Received: August 22, 2013
Accepted: October 18, 2013
Published: October 18, 2013

date, these GO or graphene based NCs are mainly prepared by using GO nanosheets as the starting seed material for in situ nanoparticle synthesis[33] or by van der Waals interactions between metal NPs with graphene.[34] Among them, GO-Ag NCs displaying superior antibacterial activity have drawn great interest from researchers even though their antibacterial mechanism is still under debate.[35−43] However, current studies on GO-Ag based NCs mainly focus on their high antibacterial property, while the stability of silver, which is the most vital factor influencing their antibacterial property and potential environmental safety, has not been carefully investigated.

The use of a magnetic component such as Fe_3O_4 or Fe_2O_3 along with Ag NPs in a composite form has been explored by many groups for easy separation and recycling purposes.[44−51] Very recently, we have prepared thin amorphous Fe_2O_3 shell coated Ag core NPs and observed their enhanced antibacterial effect compared to the plain Ag NPs with the same size, shape, surface charge, and coatings.[52] These Ag@Fe_2O_3 NPs exhibited release of Ag^+ ions under ambient conditions, which may hinder their long-term use as an efficient bactericide. Inspired by the recent studies using graphene and its derivative GO to stabilize metal surface and nanoparticles,[53−55] herein we report the preparation of Ag@Fe_2O_3-GO nanocomposites with slow Ag^+ ions release rate and long-term antibacterial property.

Core−shell Ag@Fe_2O_3 NPs were first synthesized and dispersed in hexane following our previous report,[52] and then hydrophilic GO nanosheets containing massive hydrophilic hydroxyl and carboxyl groups on its surface were utilized as a phase transfer agent,[56] where hydroxyl groups in 1-dodecanol coordinated with Ag@Fe_2O_3 NPs were replaced by abundant hydroxyl and carboxyl groups on GO. This method has several advantages compared to other approaches for GO-NPs preparation: (1) The uniform size and excellent property from NPs synthesized in oil phase can be well maintained; (2) it is a simple and general way to prepare GO based nanocomposites with NPs having strong affinity to carboxyl or hydroxyl groups; (3) NP loading density on GO can be tuned by controlling reaction time between two immiscible phases; and (4) unreacted NPs which remained in the organic phase can be easily recycled and reused.

Relative stabilities of Ag@Fe_2O_3 and its GO composites were investigated by observing nanomaterials morphology changes and monitoring their UV−vis absorption spectra, and the results showed that nanocomposites displayed very few hollow structures, unlike the case for Ag@Fe_2O_3 only. Furthermore, ion selective Ag/S composite electrode was used to detect Ag^+ ions release after dialyzing the respective nanomaterials against fresh water over 19 days. In agreement with the morphological observations, Ag@Fe_2O_3-GO displayed slower Ag^+ ions release rate compared to Ag@Fe_2O_3, indicating GO can inhibit Ag^+ release. In other words, Ag@Fe_2O_3-GO is more stable than Ag@Fe_2O_3. We then carefully compared the antibacterial property of Ag, Ag@Fe_2O_3, and Ag@Fe_2O_3-GO using Gram-negative bacteria *Escherichia coli* (*E. coli*) and Gram-positive bacteria *Bacillus subtilis* (*B. subtilis*) as model microorganisms. The Ag@Fe_2O_3-GO nanocomposites showed better long-term antibacterial property compared to Ag and Ag@Fe_2O_3 NPs. In addition to the above results, an interesting phenomenon was observed in Ag@Fe_2O_3-GO NCs during the Ag^+ release process. Recrystallized silver NPs were seen on GO nanosheets, while no similar effect was observed in the Ag@Fe_2O_3 sample. This indicates that other than slowing down oxidation of Ag to Ag^+, GO can also serve as nucleation sites for Ag deposition, which further diminished Ag^+ release into the environment.

2. EXPERIMENTAL SECTION

2.1. Synthesis of GO Nanosheets. Graphene oxide was prepared from natural graphite flake by a modified Hummers method as originally presented by Kovtyukhova et al.[57,58] Natural graphite flake (6 g) was mixed with concentrated H_2SO_4 (30 mL), $K_2S_2O_8$ (5 g), and P_2O_5 (5 g) and then incubated at 80 °C for 10 h to preoxidize the graphite. After cooling to room temperature, the reaction mixture was diluted by H_2O (1 L) and stirred for another 10 h. With three times filtering through 0.2 μm pore size polytetrafluoroethylene Millipore filter membrane and washing with distilled water until neutral pH, preoxidized graphite can be gathered and then dried in air at ambient temperature overnight. This preoxidized graphite powder (3 g) was then put into cold (below 20 °C) concentrated H_2SO_4 (120 mL), with $KMnO_4$ (15 g) added gradually with stirring and cooling. The mixture was then stirred at 35 °C for 2 h, followed by the addition of distilled water (250 mL), and stirring was continued for another 2 h. Distilled water (700 mL) was then added to terminate the reaction. Subsequently, 30% H_2O_2 (20 mL) was added in slowly and the reaction continued for 4 h with rapid stirring, after which the color of the mixture finally changed to bright yellow. The reaction mixture was centrifuged and the supernatant was discarded. The obtained precipitate was washed with 10% HCl solution three times to remove residual metal ions. To exfoliate the oxidized graphite, the obtained product was further ultrasonicated for 30 min, followed by centrifuging at 12 000 rpm for 30 min, and the exfoliated GO was collected from the supernatant. The as prepared GO can be stably dispersed in water for several months.

2.2. Preparation of Ag@Fe_2O_3-GO. Hydrophobic Ag and Ag@Fe_2O_3 NPs were first synthesized according to the procedures reported in our previous work.[52] The corresponding water-soluble NPs were obtained by using polydopamine coating through ligand exchange.

Ag@Fe_2O_3-GO NCs were obtained by phase transfer using GO as the anchoring substrate. Hydrophobic Ag@Fe_2O_3 NPs (0.5 mL) were diluted into 3 mL of hexane and then mixed with aqueous GO solution (1 mg/mL, 5 mL) with constant stirring at room temperature. The phase transfer process could be easily terminated by stopping the mixing of two immiscible phases. Unreacted NPs which still remained in hexane phase can be easily recycled and reused. The as obtained Ag@Fe_2O_3-GO NCs were washed with isopropyl alcohol (IPA) for three times to remove impurities, which were then redispersed in water.

2.3. Characterization. UV−vis absorption spectra were recorded on a Lambda-25 spectrometer (PerkinElmer, USA), and Fourier transform infrared (FTIR) spectra were recorded on a Nicolet spectrometer (Nicolet 6700, Thermo Fisher Scientific). TEM samples were prepared by drying a drop of solution in a dark room on amorphous carbon-coated nickel grids. TEM characterization was performed on a Tecnai G2 F20 S-Twin TEM (FEI, USA) operating at 200 kV. Ag concentrations in NPs and NCs were determined by first dissolving them in 5.0% aqueous HNO_3 solution and then measuring by an Inductively Coupled Plasma Optical Emission Spectrometer (PerkinElmer ICP-OES 2100 DV). Released Ag^+ ions from NPs or NCs was measured by Ag/S composite electrodes (Ruosull Technology, China) connected to a PB-10 digital pH meter (Sartorius, Germany). The optical absorption of bacterial suspensions distributed in the 96-well plate was recorded by a VICTOR X4Multilabel Plate Reader (PerkinElmer, USA).

2.4. Antibacterial Activity. Gram-negative bacteria *E. coli* or Gram-positive bacteria *B. subtilis* were incubated in Mueller-Hinton broth medium in a shaking incubator at 37 °C overnight to obtain the isolated colonies. Then, the bacteria colonies were solubilized in 0.85% (w/v) saline solution and adjusted to the 0.5 index of the MacFarland scale (1.5×10^8 colony-forming units (CFU)/mL). The bacteria were reinoculated after being properly diluted in Mueller-Hinton broth medium and distributed in a 96-well plate at the density of 10^5 CFU/well. Each well was filled by 100 μL of solution with different

concentrations of NPs or NCs. The mixture was incubated at 37 °C for 18 h, and the optical density at 595 nm was then measured to evaluate the antibacterial activity. All measurements were performed in triplicates.

2.5. Ag^+ Ions Release Rate Evaluation. The content of Ag in $Ag@Fe_2O_3$ and $Ag@Fe_2O_3$-GO solution were quantified and set at 200 ppm (mg/L) to ensure the same initial Ag concentration for Ag^+ ions release evaluation. A total of 10 mL of $Ag@Fe_2O_3$ or $Ag@Fe_2O_3$-GO solution was put into dialysis bags (MWCO 7000) and immersed in a beaker with 100 mL of ultrapure water, which was changed every day. Ag^+ ions release rate was then measured by inserting an ion selective Ag/S composite electrode into the beaker, where the potential recorded by a connected ion meter corresponded to the Ag^+ concentration. The calibration curve of potential vs Ag^+ ions concentration was acquired by measuring the potential of Ag^+ ions from standard $AgNO_3$ solutions of different concentrations.

3. RESULTS AND DISCUSSION

3.1. Nanocomposites Synthesis and Characterization. Previously, monodisperse hydrophobic $Ag@Fe_2O_3$ NPs were synthesized via a one-pot seeded growth method and then transferred into water by using dopamine. As GO based nanocomposites have shown some interesting synergic effects,[59] we propose a facile and eco-friendly method to prepare $Ag@Fe_2O_3$-GO nanocomposites. Abundant hydrophilic hydroxyl and carboxyl groups on GO can easily coordinate with metals and metal oxides.[60] In this work, 1-dodecanol coordinated with $Ag@Fe_2O_3$ can be readily replaced by GO through a ligand exchange process, as illustrated in Figure 1. The ligand exchange during the two-phase reaction

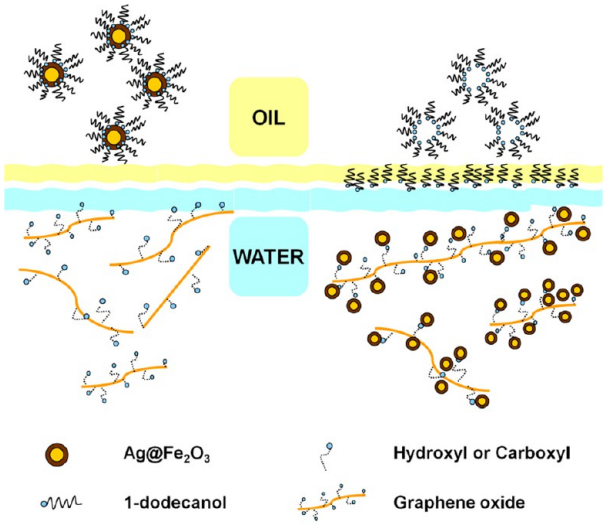

Figure 1. Schematic illustration of the formation of $Ag@Fe_2O_3$-GO nanocomposites through a phase transfer method.

was characterized by FTIR measurement, as shown in Figure 2A. The absorption peaks between 3500 cm^{-1} and 3000 cm^{-1} from GO can be assigned to O−H stretching vibrations of hydroxyl groups on GO. There are also plenty oxygen-containing functional groups, such as carboxyl COO^- (1650 cm^{-1} and 1400 cm^{-1}) and alkoxyl C−O (1100 cm^{-1}) groups observed on GO nanosheets. The spectra between 3500 cm^{-1} and 3000 cm^{-1} of $Ag@Fe_2O_3$ also indicate the existence of hydroxyl groups and likely came from the 1-dodecanol surfactant used in the synthesis. The peak at 1380 cm^{-1} shows the existence of long chain alkyl groups, which disappeared after phase transfer, indicating 1-dodecanol was

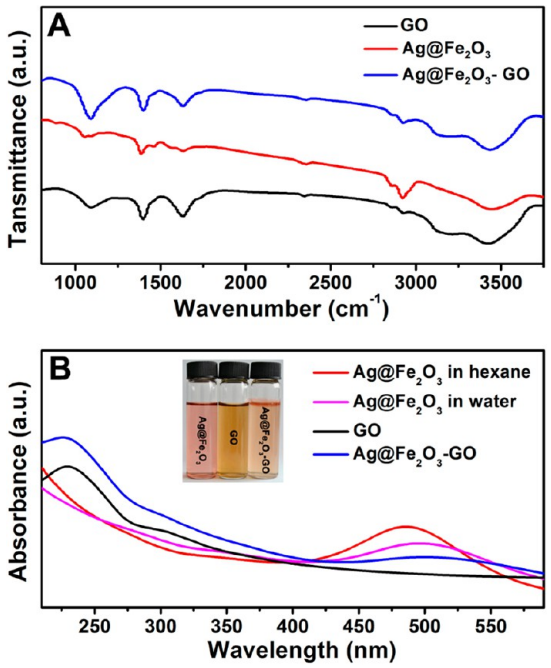

Figure 2. (A) FTIR spectra of GO, $Ag@Fe_2O_3$ and $Ag@Fe_2O_3$-GO. (B) UV−vis absorption spectra of $Ag@Fe_2O_3$ dispersed in hexane, and $Ag@Fe_2O_3$, GO, and $Ag@Fe_2O_3$-GO dispersed in water, respectively; the inset shows the color photograph of $Ag@Fe_2O_3$ dispersed in hexane and GO and $Ag@Fe_2O_3$-GO dispersed in water, respectively.

replaced by GO on the $Ag@Fe_2O_3$ surface. Figure 2B shows the UV−vis absorption spectra of GO, $Ag@Fe_2O_3$, and their composites. $Ag@Fe_2O_3$ had a distinct surface plasmon resonance (SPR) absorption at 478 nm in hexane, and that of dopamine coated $Ag@Fe_2O_3$ NPs dispersed in water slightly red-shifted due to the influence of the surrounding solvent. The $Ag@Fe_2O_3$-GO NCs showed a large 22 nm red-shift compared to the $Ag@Fe_2O_3$ NPs. The red-shift of the SPR peak can be attributed to the change of dielectric constant according to Mie theory. A color photograph of $Ag@Fe_2O_3$, GO, and $Ag@Fe_2O_3$-GO is shown in Figure 2B, inset. The magenta $Ag@Fe_2O_3$ solution changed to yellowish-red $Ag@Fe_2O_3$-GO after GO coordination. The property of GO before and after loading $Ag@Fe_2O_3$ was evaluated by Raman spectroscopy, and no obvious changes of characteristic GO Raman peaks were observed as shown in Supporting Information Figure S1.

This phase transfer method allows tuning the loading density (ratio of NPs to GO) by simply adjusting the stirring time, that is, the reaction time between NP and GO across the oil−water phase boundary. As the intensity of characteristic SPR peak in UV−vis absorption spectra is in direct proportion to the concentration of NPs, we characterized nanocomposites absorption after different reaction times. Figure 3A shows the UV−vis absorption spectra of $Ag@Fe_2O_3$-GO NCs obtained at different mixing time points. As characteristic absorption of GO is at 230 nm from the $\pi-\pi^*$ transition of the sp^2 carbon,[61,62] while that of $Ag@Fe_2O_3$ is at 500 nm, the ratio of absorbance at 500 nm to that at 230 nm reflects the loading density of NPs. Figure 3B−D are the TEM images of the NCs after different mixing times. As expected, with increasing stirring time, the density of NPs on GO increased significantly. This increased NP loading density can be displayed in a more visible way by software processing of the obtained TEM images (Figure 3E−G), where the red dots correspond to $Ag@Fe_2O_3$ NPs. The red

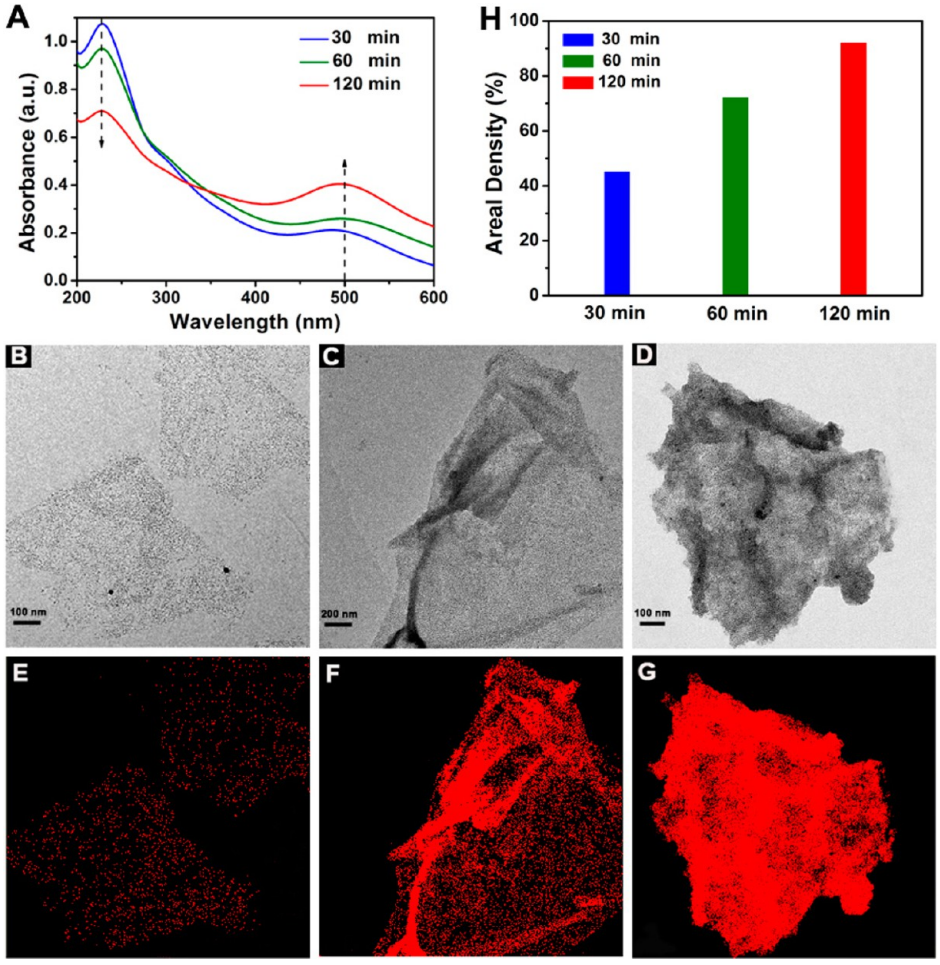

Figure 3. (A) UV−vis absorption spectra of Ag@Fe_2O_3-GO after different stirring time and corresponding TEM images of the nanocomposites after (B) 30 min, (C) 60 min, and (D) 120 min of stirring. (E−G) are contrast images of (B−D) obtained by Image-pro plus software processing, where red dots represent Ag@Fe_2O_3 NPs loaded on GO nanosheets. (H) Calculated NPs' loading density on GO after different stirring time.

areas turned larger and more agglomerative as stirring time increased, indicating more and more Ag@Fe_2O_3 NPs became anchored on GO, and more than 90% area of the GO surface was occupied after only 2 h of stirring. The measured NPs' areal densities on GO after different stirring time is displayed in Figure 3H.

3.2. Stability and Ag^+ Ions Release Property. Instability of Ag-based bactericides can limit their applications, and the main influencing factor is that Ag can be readily oxidized to Ag^+, leading to inefficiency after long-term storage and causing environmental hazard. The initial structures of the synthesized Ag@Fe_2O_3 NPs have a Ag core coated by a ~2 nm amorphous Fe_2O_3 shell.[52] For bioapplications, water-soluble Ag@Fe_2O_3 NPs (Figure 4A) could be obtained by using polydopamine which binds strongly to metal and metal oxide surfaces. Despite their excellent antibacterial property, these water-soluble Ag@Fe_2O_3 NPs suffered from the instability problem which might limit their long-term antibacterial usage, as more and more hollow Fe_2O_3 appeared as time went by (Figure 4B).

Stability of Ag@Fe_2O_3 NPs improved greatly after loading them onto GO nanosheets. In Figure 5A, an overview image of Ag@Fe_2O_3-GO shows high loading density of NPs on GO. The HRTEM image in Figure 5B demonstrates the well preserved structure and morphology of Ag@Fe_2O_3 after they were loaded on GO. More importantly, the stability of Ag@Fe_2O_3 NPs gained significant improvement owning to the interaction

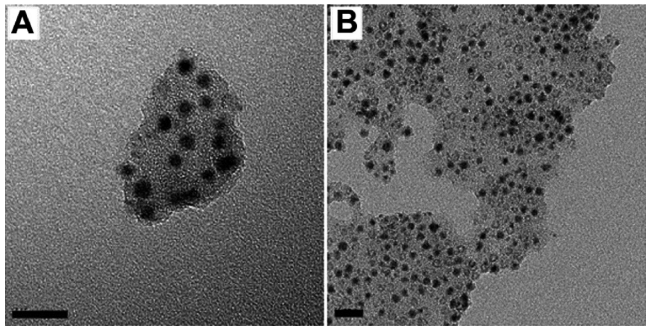

Figure 4. TEM images of polydopamine coated Ag@Fe_2O_3 NPs dispersed in water (A) and after 7 days of storage (B). All the scale bars represent 20 nm.

between them and GO. There were hardly any hollow structures as seen from Figure 5C and 5D, after they were stored under ambient environment for 7 days, in stark contrast to the scenario displayed in Figure 4B. Although still not well understood, several factors can lead to the relatively higher stability of Ag after GO was introduced into the system. For instance, oxygen containing functional groups could remove the reactive oxygen intermediates from the environment which can otherwise oxidize Ag.[63] In addition, negatively charged GO can also impede the oxidation reaction by absorbing protons that

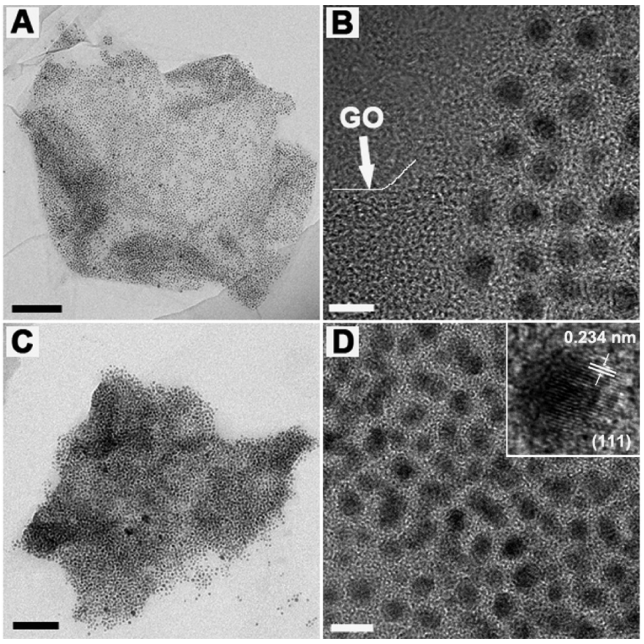

Figure 5. (A) TEM and (B) HRTEM images of Ag@Fe_2O_3-GO NCs. (C) TEM and (D) HRTEM images of Ag@Fe_2O_3-GO NCs after 7 days of storage. The black scale bars in (A) and (C) represent 100 nm, and the white scale bars in (B) and (D) represent 10 nm. The inset in (D) shows the lattice spacing of the core Ag NPs corresponding to (111) plane, and due to the amorphous nature of the Fe_2O_3 shell, it is not visible under HRTEM.

existed in the system.[56] The ability of GO and reduced graphene oxide (rGO) to stabilize Ag nanoparticles has also been utilized in surface-enhanced Raman scattering applications[53,54] and for electrochemical actuator electrode design.[55]

The measured Ag^+ ions release curve further corroborates the observed structural changes in TEM images. Shown in Figure 6, the Ag^+ release rate of the NPs is compared to that of

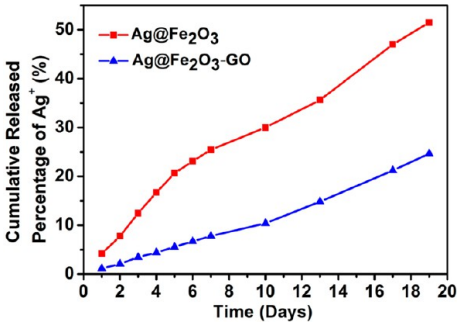

Figure 6. Ag^+ release profile after dialysis treatment, where Ag@Fe_2O_3-GO displayed a much slower Ag^+ release, especially at the beginning stage.

NCs. The measured release rate of Ag@Fe_2O_3-GO nanocomposites was two times slower than that of Ag@Fe_2O_3 nanoparticles over 19 days. During the first five days, a very small amount (~5%) of Ag^+ was released from the NCs, compared to ~20% from the NPs. After 19 days, only 25% Ag^+ (cumulative amount) was released by dialysis from NCs, while the released percentage of Ag^+ was as high as 51% for NPs. This result is another strong proof of the high stability of Ag@Fe_2O_3-GO NCs. For comparison, depending on surface coating and environment, small Ag NPs can undergo rapid dissolution, releasing more than 60% of the total Ag in the form of Ag^+ ions over a period of days[64,65] or even in hours.[66]

3.3. Synergistically Enhanced Antibacterial Property and Long-Term Efficiency. Synergistically enhanced antibacterial property was evaluated by comparing the minimum inhibitory concentrations (MICs) of Ag@Fe_2O_3 and its GO composite against Gram-negative *E. coli* and Gram-positive *B. subtilis*. For comparison, Ag was chosen as the control group. Graphene and its derivative GO/rGO have been demonstrated as efficient antibacterial materials by their specific interaction with bacterial membranes and the generation of ROS.[67,68] Under our experimental conditions, dopamine and GO showed only mild inhibition of bacteria proliferation even when their concentrations reached as high as 500 μg/mL (see Supporting Information Figure S2); thus, we neglected their role in our studies. Bacteria in broth medium without any nanomaterial addition would show a fast growth profile (Supporting Information Figure S3). As shown in Figure 7A,B, Ag@Fe_2O_3 NPs and Ag@Fe_2O_3-GO NCs exhibited enhanced antibacterial property compared to plain Ag NPs. MIC values of pure Ag NPs against *E. coli* and *B. subtilis* were both at 150.68 μg/mL, which were about 2−4 times higher than those of Ag@Fe_2O_3 and Ag@Fe_2O_3-GO (see Table 1). The Ag@Fe_2O_3-GO displayed lower MIC than Ag@Fe_2O_3 owing to the synergistically enhanced effect. In other words, Ag@Fe_2O_3-GO NCs showed better antibacterial property than the simple sum of the two constituents. With decreasing Ag concentration, we can see in Figure 7A that OD595 of Ag@Fe_2O_3-GO NCs was significantly lower than that of Ag@Fe_2O_3 NPs. This phenomenon illustrated that less *E. coli* grew in broth medium containing Ag@Fe_2O_3-GO. Although the antibacterial property against *B. subtilis* was not as good as that against *E. coli* (Figure 7B), the MIC value also indicated their slightly better antibacterial property compared to Ag@Fe_2O_3. Their long-term antibacterial properties were also studied and compared after 19 days of dialysis treatment (Figure 7C,D).

The long-term antibacterial properties of our nanoparticles and nanocomposites were evaluated after they were subjected to dialysis treatment, with the quantitative initial Ag content in Ag@Fe_2O_3 and Ag@Fe_2O_3-GO used; that is, we disregarded the Ag contents released during the dialysis process. Long-term inhibitory concentration (L-MIC) is defined as the minimum initial Ag concentration required in the nanoparticle or nanocomposite which can still completely inhibit bacterial proliferation after different days of storage or dialysis treatment. As shown in Figure 7C,D, Ag@Fe_2O_3-GO displayed the best long-term antibacterial activity, while Ag NPs lost their effectiveness even when the Ag concentration reached up to 600 μg/mL. This is likely due to the near total dissolution of small Ag nanoparticle under dialysis treatment with no cross-linked surface protections (see Supporting Information Figure S4).[66] Ag@Fe_2O_3 L-MIC values against *E. coli* and *B. subtilis* were both at 290.44 μg/mL, while Ag@Fe_2O_3-GO L-MIC against *E. coli* was only 71.71 μg/mL (143.43 μg/mL against *B. subtilis*). These values are consistent with the observed trend of the Ag^+ ion release profile, as the nanocomposites showed the suppressed release of Ag^+ and thus increased core Ag nanoparticle long-term stability. There are some uncertainties in determining the exact MIC values due to the method we adopted here using serial dilution of the nanomaterials.

3.4. Recrystallization of Ag on GO. As shown in Supporting Information Figure S5, after 19 days dialysis,

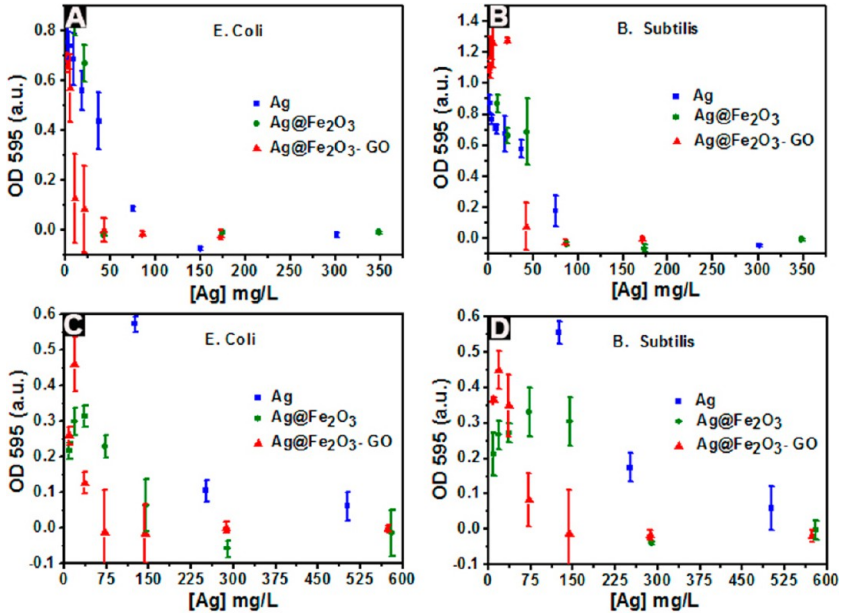

Figure 7. Antibacterial activities against (A) *E. coli* and (B) *B. subtilis* evaluated by measuring optical density at 595 nm after 18 h of incubation with different concentrations of Ag, Ag@Fe_2O_3, and Ag@Fe_2O_3-GO nanomaterials at 37 °C. Minimum inhibitory concentrations (MIC) were the minimum concentrations that completely inhibited bacterial growth (where OD595 dropped to zero). (C, D) After 19 days of dialysis, Ag, Ag@Fe_2O_3, and Ag@Fe_2O_3-GO were again incubated with the bacteria strains under the same conditions. Long-term minimum inhibitory concentrations (L-MIC) were similarly determined by the concentrations (initial Ag concentration before dialysis treatment) that completely inhibited bacterial growth. All the MIC values presented here were the initial concentration of Ag in the nanomaterials determined by ICP-OES. The error bars represent standard deviations of the measurements (n = 3).

Table 1. Minimum Inhibitory Concentrations (MIC) and Long-Term MIC (L-MIC) of Ag, Ag@Fe_2O_3, and Ag@Fe_2O_3-GO against *E. coli* and *B. subtilis*

MIC (μg/mL)	*E. coli*	*B. subtilis*
Ag	150.68	150.68
Ag@Fe_2O_3	43.57	87.13
Ag@Fe_2O_3-GO	43.03	86.06
L-MIC (μg/mL)	*E. coli*	*B. subtilis*
Ag	NA	NA
Ag@Fe_2O_3	290.44	290.44
Ag@Fe_2O_3-GO	71.71	143.43

some large Ag was seen recrystallized on GO, with irregular sizes up to 60 nm. Such a phenomenon was not observed for Ag@Fe_2O_3 NPs. Ag^+ ions released from the core Ag NPs were likely reduced again by mild reductants in the solution or via a photochemical process, forming Ag NPs on the GO surface.[12,69] UV−vis absorption spectra also reflected the difference of two materials during the release process. As shown in Supporting Information Figure S6A,B, absorbance of Ag@Fe_2O_3 at 496 nm decreased over time indicating that its concentration was decreasing, while recrystallized Ag NPs resulted in blue-shift and broadening of Ag@Fe_2O_3-GO SPR absorption (Supporting Information Figure S6C,D). Such a phenomenon was not observed in the absence of GO (Supporting Information Figure S6B). As Ag NPs recrystallization effectively reduces Ag^+ release into the surrounding environment, this effect also contributes to the observed suppressed Ag^+ release and sustained long-term antibacterial property.

The disappearance of the characteristic GO absorption peak at 230 nm in Supporting Information Figure S6C was likely due to the interaction of recrystallized Ag with GO. The $\pi-\pi^*$ transition of GO depends on the conjugative effect related to its nanometer-scale sp^2 clusters, which might be affected by electronic interaction with Ag nanoparticles or GO itself as in a aggregated form.[62] We have investigated the absorbance change of GO by forming composite with Ag NPs and salt induced aggregation (Supporting Information Figure S7), and both experiments showed decreased $\pi-\pi^*$ transition of GO, with Ag-GO showing almost a vanishing 230 nm absorption peak, similar to what was observed in Supporting Information Figure S6C.

4. CONCLUSIONS

In summary, we have investigated synthetic mechanism and long-term antibacterial activity of Ag@Fe_2O_3-GO nanocomposites by developing a facile ligand exchange method, where nanoparticle loading density on GO can be easily tuned. The abundant hydroxyl and carboxyl groups on GO served as the anchoring point for Ag@Fe_2O_3 NPs, replacing the originally coordinated 1-dodecanol molecules. We have found that the as formed water-soluble Ag@Fe_2O_3-GO NCs were more stable than Ag@Fe_2O_3 NPs by carefully monitoring their morphology changes under TEM and the Ag^+ release curves. After long-term storage, many hollow structured Fe_2O_3 NPs were observed in Ag@Fe_2O_3 NPs, which were rarely seen in Ag@Fe_2O_3-GO NCs. The measured Ag^+ release curves also showed that Ag@Fe_2O_3 exhibited about two times higher release rate than that of Ag@Fe_2O_3-GO NCs over a 19 day period. Antibacterial experiments showed that Ag@Fe_2O_3-GO displayed synergistically enhanced antibacterial property and longer-term antibacterial efficiency compared to Ag and Ag@Fe_2O_3. The suppressed oxidation of Ag and Ag recrystallization on GO contributed to the slow Ag^+ ions release and long-term antibacterial activity for Ag@Fe_2O_3-GO nanocomposites. Our study demonstrates that the surface and interface between Ag

and Fe_2O_3, as well as Ag@Fe_2O_3 to GO nanosheets, play important roles in the chemical stability of Ag nanoparticles and subsequently their antibacterial properties, which should be valuable for future design of highly efficient nanomaterials-based bactericide with long-term stability and low environmental hazard.

■ ASSOCIATED CONTENT

Supporting Information

Raman spectra of GO before and after NP loading, bacteria proliferation curve and the inhibition effect of GO, Ag^+ release profile from Ag nanoparticles, TEM images of Ag@Fe_2O_3-GO after dialysis, and UV−vis absorption spectra of Ag@Fe_2O_3 and Ag@Fe_2O_3-GO after storage, and absorption spectra of Ag-GO and GO aggregates. This material is available free of charge via the Internet at http://pubs.acs.org.

■ AUTHOR INFORMATION

Corresponding Author

*E-mail: jjiang2010@sinano.ac.cn.

Author Contributions

The manuscript was written through contributions of all authors. All authors have given approval to the final version of the manuscript.

Notes

The authors declare no competing financial interest.

■ ACKNOWLEDGMENTS

This work is funded by the "Hundred Talents" program of Chinese Academy of Sciences, and Natural Science Foundation of China (Grant 21175148). The bacterial strains are kindly provided by Dr. Mingzhe Gan at SINANO, and the graphene oxide samples are generously given by Guan Wu at SINANO.

■ REFERENCES

(1) Seil, J. T.; Webster, T. J. *Int. J. Nanomed.* **2012**, *7*, 2767−2781.
(2) Chernousova, S.; Epple, M. *Angew. Chem., Int. Ed.* **2013**, *52*, 1636−1653.
(3) Chaloupka, K.; Malam, Y.; Seifalian, A. M. *Trends Biotechnol.* **2010**, *28*, 580−588.
(4) Yuan, X.; Setyawati, M. I.; Tan, A. S.; Ong, C. N.; Leong, D. T.; Xie, J. *NPG Asia Mater.* **2013**, *5*, e39.
(5) Xiu, Z. M.; Zhang, Q. B.; Puppala, H. L.; Colvin, V. L.; Alvarez, P. J. *Nano Lett.* **2012**, *12*, 4271−4275.
(6) Yang, X.; Gondikas, A. P.; Marinakos, S. M.; Auffan, M.; Liu, J.; Hsu-Kim, H.; Meyer, J. N. *Environ. Sci. Technol.* **2012**, *46*, 1119−1127.
(7) Amato, E.; Diaz-Fernandez, Y. A.; Taglietti, A.; Pallavicini, P.; Pasotti, L.; Cucca, L.; Milanese, C.; Grisoli, P.; Dacarro, C.; Fernandez-Hechavarria, J. M.; Necchi, V. *Langmuir* **2011**, *27*, 9165−9173.
(8) Taglietti, A.; Diaz Fernandez, Y. A.; Amato, E.; Cucca, L.; Dacarro, G.; Grisoli, P.; Necchi, V.; Pallavicini, P.; Pasotti, L.; Patrini, M. *Langmuir* **2012**, *28*, 8140−8148.
(9) Yin, L.; Cheng, Y.; Espinasse, B.; Colman, B. P.; Auffan, M.; Wiesner, M.; Rose, J.; Liu, J.; Bernhardt, E. S. *Environ. Sci. Technol.* **2011**, *45*, 2360−2367.
(10) Morones, J. R.; Elechiguerra, J. L.; Camacho, A.; Holt, K.; Kouri, J. B.; Ramírez, J. T.; Yacaman, M. J. *Nanotechnology* **2005**, *16*, 2346−2353.
(11) Choi, O.; Hu, Z. *Environ. Sci. Technol.* **2008**, *42*, 4583−4588.
(12) Glover, R. D.; Miller, J. M.; Hutchison, J. E. *ACS Nano* **2011**, *5*, 8950−8957.
(13) Varela-Rizo, H.; Martín-Gullón, I.; Terrones, M. *ACS Nano* **2012**, *6*, 4565−4572.
(14) Tian, J.; Liu, S.; Zhang, Y.; Li, H.; Wang, L.; Luo, Y.; Asiri, A. M.; Al-Youbi, A. O.; Sun, X. *Inorg. Chem.* **2012**, *51*, 4742−4746.
(15) Wang, H.; Yang, Y.; Liang, Y.; Robinson, J. T.; Li, Y.; Jackson, A.; Cui, Y.; Dai, H. *Nano Lett.* **2011**, *11*, 2644−2647.
(16) Liang, Y.; Li, Y.; Wang, H.; Zhou, J.; Wang, J.; Regier, T.; Dai, H. *Nat. Mater.* **2011**, *10*, 780−786.
(17) Zhu, M.; Chen, P.; Liu, M. *ACS Nano* **2011**, *5*, 4529−4536.
(18) Guo, S.; Zhang, S.; Wu, L.; Sun, S. *Angew. Chem., Int. Ed.* **2012**, *51*, 11770−11773.
(19) Wang, H.; Liang, Y.; Li, Y.; Dai, H. *Angew. Chem., Int. Ed.* **2011**, *50*, 10969−10972.
(20) Wu, Z.-S.; Yang, S.; Sun, Y.; Parvez, K.; Feng, X.; Müllen, K. *J. Am. Chem. Soc.* **2012**, *134*, 9082−9085.
(21) Dong, X.; Huang, W.; Chen, P. *Nanoscale Res. Lett.* **2011**, *6*, 60.
(22) Luo, Z.; Yuwen, L.; Han, Y.; Tian, J.; Zhu, X.; Weng, L.; Wang, L. *Biosens. Bioelectron.* **2012**, *36*, 179−185.
(23) Myung, S.; Solanki, A.; Kim, C.; Park, J.; Kim, K. S.; Lee, K.-B. *Adv. Mater.* **2011**, *23*, 2221−2225.
(24) Liu, Z.; Robinson, J. T.; Sun, X.; Dai, H. *J. Am. Chem. Soc.* **2008**, *130*, 10876−10877.
(25) Zhang, L.; Xia, J.; Zhao, Q.; Liu, L.; Zhang, Z. *Small* **2010**, *6*, 537−544.
(26) Jung, J. H.; Cheon, D. S.; Liu, F.; Lee, K. B.; Seo, T. S. *Angew. Chem., Int. Ed.* **2010**, *49*, 5708−5711.
(27) Robinson, J. T.; Tabakman, S. M.; Liang, Y.; Wang, H.; Sanchez Casalongue, H.; Vinh, D.; Dai, H. *J. Am. Chem. Soc.* **2011**, *133*, 6825−6831.
(28) Yang, K.; Feng, L.; Shi, X.; Liu, Z. *Chem. Soc. Rev.* **2013**, *42*, 530−547.
(29) Liu, J.; Fu, S.; Yuan, B.; Li, Y.; Deng, Z. *J. Am. Chem. Soc.* **2010**, *132*, 7279−7281.
(30) Peng, E.; Choo, E. S.; Chandrasekharan, P.; Yang, C. T.; Ding, J.; Chuang, K. H.; Xue, J. M. *Small* **2012**, *8*, 3620−3630.
(31) Zhou, X.; Huang, X.; Qi, X.; Wu, S.; Xue, C.; Boey, F. Y. C.; Yan, Q.; Chen, P.; Zhang, H. *J. Phys. Chem. C* **2009**, *113*, 10842−10846.
(32) Cui, S.; Mao, S.; Lu, G.; Chen, J. *J. Phys. Chem. Lett.* **2013**, *4*, 2441−2454.
(33) Pang, D. W.-P.; Yuan, F.-W.; Chang, Y.-C.; Li, G.-A.; Tuan, H.-Y. *Nanoscale* **2012**, *4*, 4562−4570.
(34) Wang, X.; Meng, G.; Zhu, C.; Huang, Z.; Qian, Y.; Sun, K.; Zhu, X. *Adv. Funct. Mater.* **2013**, DOI: 10.1002/adfm.201301409, (online early access).
(35) Ma, J.; Zhang, J.; Xiong, Z.; Yong, Y.; Zhao, X. S. *J. Mater. Chem.* **2011**, *21*, 3350−3352.
(36) Pasricha, R.; Gupta, S.; Srivastava, A. K. *Small* **2009**, *5*, 2253−2259.
(37) Shen, J.; Shi, M.; Li, N.; Yan, B.; Ma, H.; Hu, Y.; Ye, M. *Nano Res.* **2010**, *3*, 339−349.
(38) Bao, Q.; Zhang, D.; Qi, P. *J. Colloid Interface Sci.* **2011**, *360*, 463−470.
(39) Li, C.; Wang, X.; Chen, F.; Zhang, C.; Zhi, X.; Wang, K.; Cui, D. *Biomaterials* **2013**, *34*, 3882−3890.
(40) Liu, L.; Liu, J.; Wang, Y.; Yan, X.; Sun, D. D. *New J. Chem.* **2011**, *35*, 1418−1423.
(41) Tang, J.; Chen, Q.; Xu, L.; Zhang, S.; Feng, L.; Cheng, L.; Xu, H.; Liu, Z.; Peng, R. *ACS Appl. Mater. Interfaces* **2013**, *5*, 3867−3874.
(42) Xu, W.-P.; Zhang, L.-C.; Li, J.-P.; Lu, Y.; Li, H.-H.; Ma, Y.-N.; Wang, W.-D.; Yu, S.-H. *J. Mater. Chem.* **2011**, *21*, 4593−4597.
(43) Zhang, Z.; Zhang, J.; Zhang, B.; Tang, J. *Nanoscale* **2013**, *5*, 118−123.
(44) Gong, P.; Li, H.; He, X.; Wang, K.; Hu, J.; Tan, W.; Zhang, S.; Yang, X. *Nanotechnology* **2007**, *18*, 285604.
(45) Prucek, R.; Tuček, J.; Kilianová, M.; Panáček, A.; Kvítek, L.; Filip, J.; Kolář, M.; Tománková, K.; Zbořil, R. *Biomaterials* **2011**, *32*, 4704−4713.
(46) Wei, Z.; Zhou, Z.; Yang, M.; Lin, C.; Zhao, Z.; Huang, D.; Chen, Z.; Gao, J. *J. Mater. Chem.* **2011**, *21*, 16344−16348.

(47) Chudasama, B.; Vala, A. K.; Andhariya, N.; Upadhyay, R. V.; Mehta, R. V. *J. Magn. Magn. Mater.* **2011**, *323*, 1233−1237.
(48) Zhang, X. L.; Niu, H. Y.; Yan, J. P.; Cai, Y. Q. *Colloids Surf., A* **2011**, *375*, 186−192.
(49) Liu, J.; Zhao, Z.; Feng, H.; Cui, F. *J. Mater. Chem.* **2012**, *22*, 13891−13894.
(50) Park, H. H.; Park, S.; Ko, G.; Woo, K. *J. Mater. Chem. B* **2013**, *1*, 2701−2709.
(51) Zhai, Y.; Han, L.; Wang, P.; Li, G.; Ren, W.; Liu, L.; Wang, E.; Dong, S. *ACS Nano* **2011**, *5*, 8562−8570.
(52) Chen, Y.; Gao, N.; Jiang, J. *Small* **2013**, *9*, 3242−3246.
(53) Kim, Y.-K.; Han, S. W.; Min, D.-H. *ACS Appl. Mater. Interfaces* **2012**, *4*, 6545−6551.
(54) Murphy, S.; Huang, L.; Kamat, P. V. *J. Phys. Chem. C* **2013**, *117*, 4740−4747.
(55) Lu, L.; Liu, J.; Hu, Y.; Zhang, Y.; Chen, W. *Adv. Mater.* **2013**, *25*, 1270−1274.
(56) Goncalves, G.; Marques, P. A. A. P.; Granadeiro, C. M.; Nogueira, H. I. S.; Singh, M. K.; Gráci, J. *Chem. Mater.* **2009**, *21*, 4796−4802.
(57) Li, D.; Müller, M. B.; Gilje, S.; Kaner, R. B.; Wallace, G. G. *Nat. Nanotechnol.* **2008**, *3*, 101−105.
(58) Kovtyukhova, N. I.; Ollivier, P. J.; Martin, B. R.; Mallouk, T. E.; Chizhik, S. A.; Buzaneva, E. V.; Gorchinskiy, A. D. *Chem. Mater.* **1999**, *11*, 771−778.
(59) Huang, X.; Qi, X.; Boey, F.; Zhang, H. *Chem. Soc. Rev.* **2012**, *41*, 666−686.
(60) Dreyer, D. R.; Park, S.; Bielawski, C. W.; Ruoff, R. S. *Chem. Soc. Rev.* **2010**, *39*, 228−240.
(61) Eda, G.; Lin, Y.-Y.; Mattevi, C.; Yamaguchi, H.; Chen, H.-A.; Chen, I. S.; Chen, C.-W.; Chhowalla, M. *Adv. Mater.* **2010**, *22*, 505−509.
(62) Lai, Q.; Zhu, S. F.; Luo, X. P.; Zou, M.; Huang, S. H. *AIP Adv.* **2012**, *2*, 032146.
(63) Goncalves, G.; Cruz, S. M. A.; Ramalho, A.; Gracio, J.; Marques, P. A. A. P. *Nanoscale* **2012**, *4*, 2937−2945.
(64) Ma, R.; Levard, C.; Marinakos, S. M.; Cheng, Y.; Liu, J.; Michel, F. M.; Brown, G. E.; Lowry, G. V. *Environ. Sci. Technol.* **2012**, *46*, 752−759.
(65) Sotiriou, G. A.; Meyer, A.; Knijnenburg, J. T. N.; Panke, S.; Pratsinis, S. E. *Langmuir* **2012**, *28*, 15929−15936.
(66) Liu, J.; Sonshine, D. A.; Shervani, S.; Hurt, R. H. *ACS Nano* **2010**, *4*, 6903−6913.
(67) Liu, S.; Zeng, T. H.; Hofmann, M.; Burcombe, E.; Wei, J.; Jiang, R.; Kong, J.; Chen, Y. *ACS Nano* **2011**, *5*, 6971−6980.
(68) Krishnamoorthy, K.; Veerapandian, M.; Zhang, L.-H.; Yun, K.; Kim, S. J. *J. Phys. Chem. C* **2012**, *116*, 17280−17287.
(69) Chen, J.; Zheng, X.; Wang, H.; Zheng, W. *Thin Solid Films* **2011**, *520*, 179−185.